Chapter-6

SELF-ORGANIZATION OF BOUNDED SOLAR PLASMA WITH NEGATIVE IONS IN GRAVITO-ELECTROSTATIC PHASE SPACE

Abstract: *The self-organization and fluid elemental dynamics in the confined solar plasma system in the GES-model fabric with realistic negative ionic species is explored illustratively. The distribution of mass and electric charge of the constituents in the SIP is studied with the spatial gradient profiles of the self-gravity and electric field, respectively. The fluid flow characteristics clearly reveal a unique type of the SIP material clumping behaviour. The positive (negative) ions are more susceptible to the region of high (low) self-gravity and low (high) electrostatic field effects. It shows that the SIP does not favour the formation of heavy negative ions (against the lighter ones). This result clearly matches with diversified astronomic results reported in the literature*[†].

6.1 INTRODUCTION

The whole solar plasma system has served as a naturally occurring complex laboratory for exploring a wide variety of plasma structurization processes. One of the most formidable and significant challenges in this endeavour involves the comprehension of the plasma elemental flow dynamics in the presence of various force field interactions. This eventually influences the spontaneous formation of structures within the solar plasma components. Existing literature widely admits successful modelling of the solar interior structure using the well-accepted standard solar model (SSM) in the past. Nonetheless, the process of plasma self-organization within the solar interior, accounting for the realistic variety of negative ionic species, remains an unexplored territory [1-3].

As a consequence, with the above-mentioned fact as the driving motivation, the present chapter is dedicated to illuminate the dynamical characteristics of the diverse plasma constituent elements in the bounded solar structure. This exploration culminates in the materialistic arrangement of the confined solar interior plasma (SIP) medium as

[†]Sarma, P. and Karmakar, P. K. Effects of negative ions on equilibrium solar plasmas in the fabric of gravito-electrostatic sheath model. *Scientific Reports*, Under Review, 2023.

per the gravito-electrostatic sheath (GES) model fabric, incorporating diverse negative ions aligning with observational predictions [4, 5].

6.2 PHYSICAL MODEL FORMULATION

The solar plasma medium is presumed to comprise lighter non-gravitating inertialess Boltzmann electrons and heavier gravitating inertial fluidic positive ions (of a single kind, i.e., H^+) and negative ions (diverse in terms of mass). The entire solar plasma system is considered to be spherically symmetric for analytical simplicity, which enables us to comprehend the 3D system as a reduced 1D one [1, 2]. The structure is supposed to be in the isothermal hydrostatic equilibrium configuration throughout the entire confined solar plasma medium. Accordingly, the model equations are carefully developed for the tri-component plasma system. The key physical insights behind the sheath formation in such solar plasma domain as explained in the previous chapters are retained here as well.

All the model governing equations are presented below in their steady normalized form. The equations here depict the bounded SIP mass. The external boundary of the confined structure is determined by the exact gravito-electrostatic force-balancing condition. This set of equations consists of the Boltzmann electron distribution function, continuity and momentum equations following the flux and linear momentum conservation respectively of the positive and negative ions, the equations of state for the positive and negative ionic species, the electro-gravitational Poisson equations depicting the respective potential structures, and the electric current density evolution equation. The significances of the symbols and the normalization scheme followed here are detailed in Tables 5.1 and 5.2 respectively. Accordingly, the equations are written below.

The normalized Boltzmann electron distribution law is expressed as

$$N_e = \exp(\Phi). \tag{6.1}$$

The dynamics of the constitutive positive ions is governed by the continuity equation, momentum equation, and the equation of state expressed respectively in the time-stationary normalized form as

$$\frac{1}{N_+}\left(\partial_\xi N_+\right)+\frac{1}{M_+}\left(\partial_\xi M_+\right)+\frac{2}{\xi}=0\,, \tag{6.2}$$

$$M_+\left(\partial_\xi M_+\right)=-\partial_\xi \Phi-\left(\frac{T_+}{T_e}\right)\frac{1}{N_+}\left(\partial_\xi N_+\right)-\partial_\xi \Psi\,, \tag{6.3}$$

$$P_{T+}^{*}=\left(\frac{n_{+0}k_BT_{+}}{P_0}\right)N_{+}. \tag{6.4}$$

The respective equations for the negative ions are depicted as

$$\frac{1}{N_{-}}\left(\partial_{\xi}N_{-}\right)+\frac{1}{M_{-}}\left(\partial_{\xi}M_{-}\right)+\frac{2}{\xi}=0, \tag{6.5}$$

$$M_{-}\left(\partial_{\xi}M_{-}\right)=\frac{m_{+}}{m_{-}}\left(\partial_{\xi}\Phi\right)-\frac{m_{+}}{m_{-}}\left(\frac{T_{-}}{T_e}\right)\frac{1}{N_{-}}\left(\partial_{\xi}N_{-}\right)-\partial_{\xi}\Psi, \tag{6.6}$$

$$P_{T-}^{*}=\left(\frac{n_{-0}k_BT_{-}}{P_0}\right)N_{-}. \tag{6.7}$$

The normalized electrostatic and gravitational Poisson equations representing the corresponding potential distribution are expressed respectively as

$$\partial_{\xi}^{2}\Phi+\frac{2}{\xi}\left(\partial_{\xi}\Phi\right)=\left(\frac{\lambda_J}{\lambda_{De}}\right)^{2}\left[(1-\delta)N_e+\delta N_{-}-N_{+}\right], \tag{6.8}$$

$$\partial_{\xi}^{2}\Psi+\frac{2}{\xi}\left(\partial_{\xi}\Psi\right)=\left[N_{+}+\delta N_{-}\right]. \tag{6.9}$$

The electric current density evolution equation in the normalized form is given as

$$J_{SIP}=N_{+}\left[-\sqrt{2\xi\left(\partial_{\xi}\Psi\right)}-\sqrt{2\xi\left(\partial_{\xi}\Phi\right)}\right]+\delta N_{-}\left[-\sqrt{2\xi\left(\partial_{\xi}\Psi\right)}+\sqrt{2\xi\left(\frac{m_{+}}{m_{-}}\right)\left(\partial_{\xi}\Phi\right)}\right]+(1-\delta)N_e\sqrt{2\xi\left(\frac{m_{+}}{m_e}\right)\left(\partial_{\xi}\Phi\right)}. \tag{6.10}$$

The equations (6.1)-(6.10) represent the steady-state dynamics of the self-gravitating SIP and the resulting equilibrium structure in the presence of the considered negative ions. The normalized equations above are now coupled to obtain a closed set of time-stationary first-order differential equations for numerical analysis. The fourth-order Runge-Kutta (RK-IV) method is applied for the analysis with the judicious initial and input values, as shown in Table 5.3, using MATLAB [6, 7]. In the subsequent analyses, we replace the positive ionic symbol "+", as in the equations, with "i", as per the usual convention.

6.3 RESULTS AND DISCUSSIONS

With the aim of exploring the steady-state organization of the confined solar plasma system with diverse negative ions, at first, the location of the new solar surface boundary (SSB) formation by an exact gravito-electrostatic force-balancing is investigated. Accordingly, the variation of the equilibrium net GES-force (defined as the algebraic sum of self-gravity and electric field) with the Jeans-normalized heliocentric radial

distance variation is depicted for the different indicated values of δ, m_i/m_-, T_i/T_e, and T_-/T_e in figure 6.1. It is found that the SSB location sensitively depends on the variation of this δ-parameter only (figure 6.1(a)), but not so significantly on other considered input parameters (figures 6.1(b)-6.1(d)). The SSB location here is quite in accordance with the basic rule of exact gravito-electrostatic force balancing mechanism, leading to the SSB formation as extensively illustrated in the literature [6, 8]. The modified SSB divides the entire solar plasma volume into a bi-scaled system, bounded (SIP) and unbounded (solar wind plasma or SWP), separated by the interfacial SSB. This complex plasma system evolves with the new quantitative variations parametrically introduced by the considered negative ionic species.

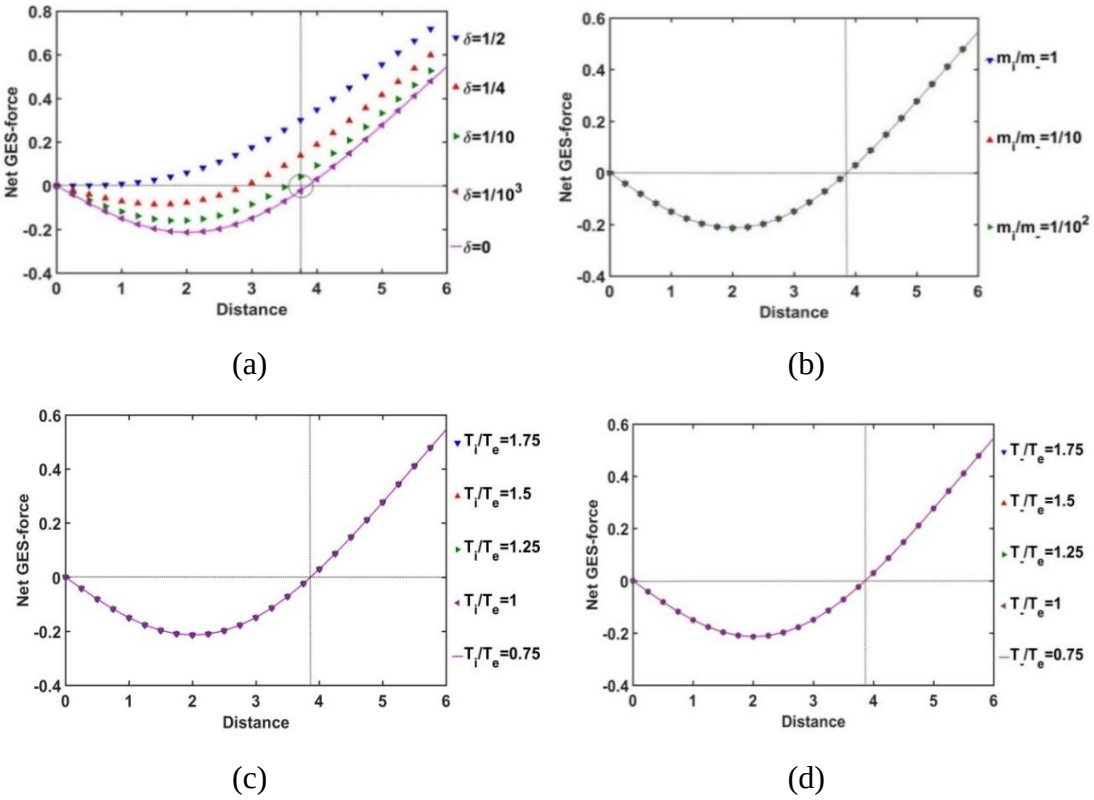

Figure 6.1: *Variation of the net GES-force with the Jeans-normalized heliocentric radial distance for different values of the (a) equilibrium negative-to-positive ion density ratio (δ) with fixed $m_i/m_-=1$, $T_i/T_e=1$ and $T_-/T_e=1$; (b) positive-to-negative ion mass ratio (m_i/m_-) with fixed $\delta=1/1000$, $T_i/T_e=1$ and $T_-/T_e=1$; (c) positive ion-to-electron temperature ratio (T_i/T_e) with fixed $\delta=1/1000$, $m_i/m_-=1$ and $T_-/T_e=1$; and (d) negative ion-to-electron temperature ratio (T_-/T_e) with fixed $\delta=1/1000$, $m_i/m_-=1$ and $T_i/T_e=1$.*

It is clear that the SSB (location of zero net GES-force) shrinks with an increase in the negative ion concentration (i.e., increase in δ-value). The physics behind is clearly explained in **Chapter-5**. Now the self-organization and the fluid element dynamical properties of the SIP constituent material are elaborately studied as follows.

In figure 6.2, the spatial variation of the normalized SIP self-gravitational field strength gradient is portrayed. It is seen from figure 6.2(a) that the non-uniformity in the self-gravity of the SIP is sensitive to the δ-variation. This self-gravity non-uniformity is higher towards the heliocentric region, which is due to higher inhomogeneity in gravitating material distribution towards the heliocentric region. It is noteworthy that the appearance of a δ-insensitive location for the self-gravity non-uniformity (i.e., a trans-critical point) is prominent at $\xi \approx 3.25$. After that location, the self-gravity gradient follows the opposite trend to that from the heliocenter to $\xi \approx 3.25$. We further speculate that the self-gravity gradient is independent of the m_i/m_-, T_i/T_e, and T_-/T_e-variation cases of the SIP medium as seen from figures 6.2(b)-6.2(d), respectively. This behaviour signifies that the radial inhomogeneity of the net gravitating matter population distribution in the SIP is insensitive to these three parameters (m_i/m_-, T_i/T_e, and T_-/T_e) above against the δ-variation scenarios of the bounded SIP medium.

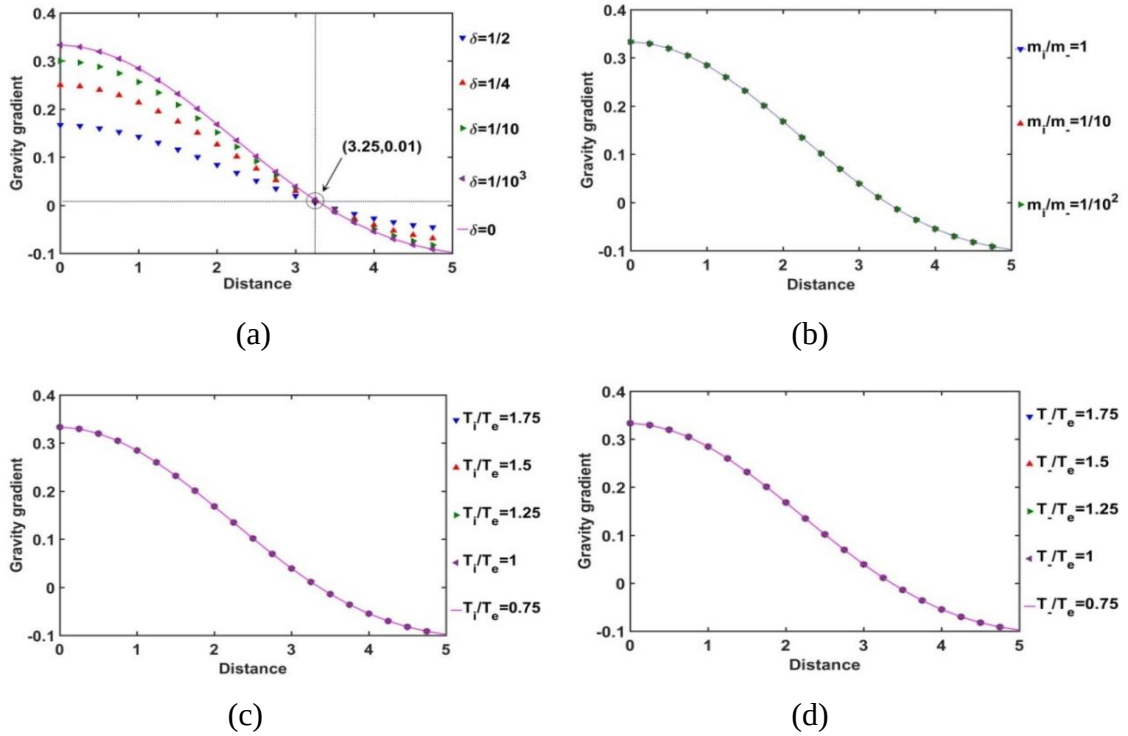

Figure 6.2: *Variation of the gradient of SIP self-gravitational field strength (gravity) with the Jeans-normalized heliocentric radial distance for different values of (a)*

equilibrium negative-to-positive ion density ratio (δ) with fixed $m_i/m_-=1$, $T_i/T_e=1$ and $T_-/T_e=1$; (b) positive-to-negative ion mass ratio (m_i/m_-) with fixed $\delta=1/1000$, $T_i/T_e=1$ and $T_-/T_e=1$; (c) positive ion-to-electron temperature ratio (T_i/T_e) with fixed $\delta=1/1000$, $m_i/m_-=1$ and $T_-/T_e=1$; and (d) negative ion-to-electron temperature ratio (T_-/T_e) with fixed $\delta=1/1000$, $m_i/m_-=1$ and $T_i/T_e=1$.

In figure 6.3, the gradient of the SIP electric field strength is plotted with the Jeans-normalized heliocentric radial distance for different values of δ (figure 6.3(a)), m_i/m_- (figure 6.3(b)), T_i/T_e (figure 6.3(c)) and T_-/T_e (figure 6.3(d)). The electric field increment is uniform throughout the SIP scale, but except near the heliocentric region. It is seen further that, from the heliocenter to $\xi \approx 0.5$, a relative decrease in the material concentration causes an increase in the electric field gradient and hence, an increase in the electric field strength; and vice-versa.

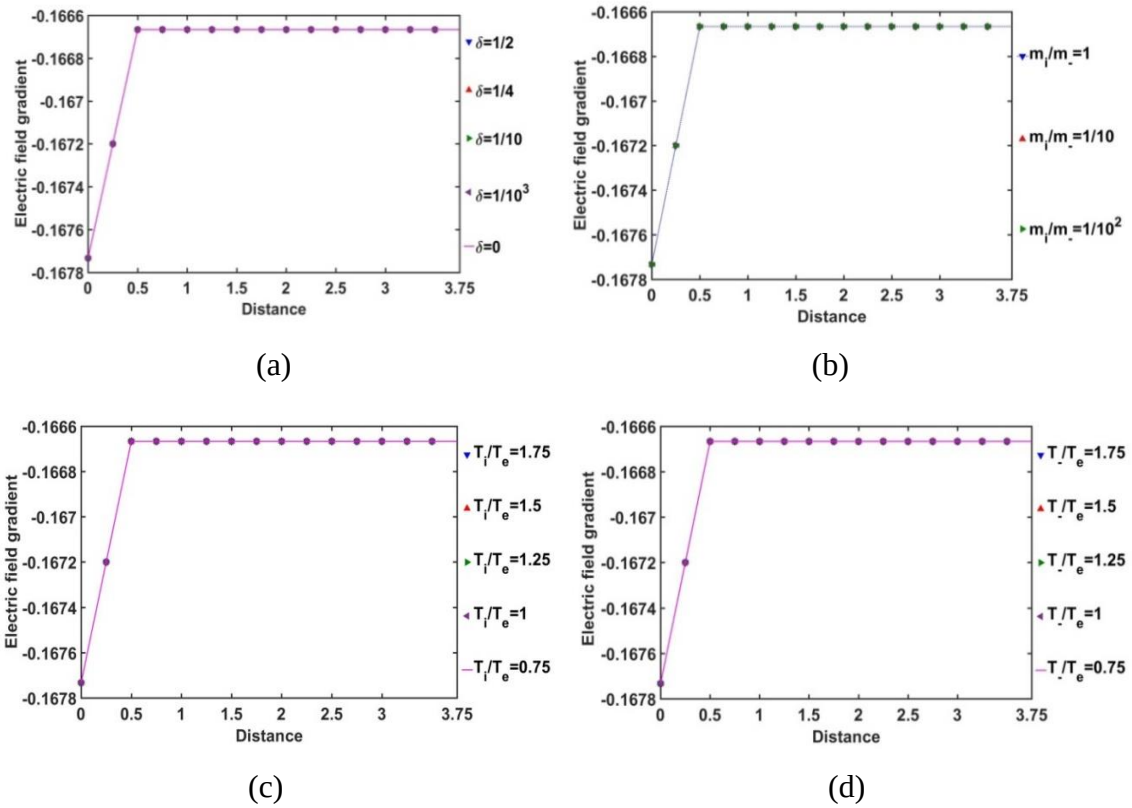

(a) (b)

(c) (d)

Figure 6.3: *Variation of the gradient of the SIP electric field strength with the Jeans-normalized heliocentric radial distance for different values of the (a) equilibrium negative-to-positive ion density ratio (δ) with fixed $m_i/m_-=1$, $T_i/T_e=1$ and $T_-/T_e=1$; (b) positive-to-negative ion mass ratio (m_i/m_-) with fixed $\delta=1/1000$, $T_i/T_e=1$ and $T_-/T_e=1$; (c)*

positive ion-to-electron temperature ratio (T_i/T_e) with fixed δ=1/1000, m_i/m_-=1 and T_-/T_e=1; and (d) negative ion-to-electron temperature ratio (T_-/T_e) with fixed δ=1/1000, m_i/m_-=1 and T_i/T_e=1. The inner distinctions of these similar profiles obviously lie in the multi-parametric variations of current solar plasma relevance as shown herein.

In figures 6.4-6.7, we portray the profile of the net SIP GES-force together with its conjugated gravito-electrostatic components (gravito-electrostatic phase space) for different values of δ (figure 6.4), m_i/m_- (figure 6.5), T_i/T_e (figure 6.6) and T_-/T_e (figure 6.7). It illustrates the 2-D flow vectors with their length and direction uniquely specifying the net GES-force vectors. The combined pattern of such vectorial flow variations in the form of 3-D graphical structures is also illustrated therein. It is interestingly seen that the dynamical behaviours of the various constituent species composing the entire SIP system with the following characteristic properties can be mapped to the distinct regions of the 2-D vector plots (figures 6.4-6.7) categorized as follows:

a) Very light but highly charged particle dynamics (the lower left region);
b) Very light neutral particle dynamics (the upper left region);
c) Very heavy and highly charged particle dynamics (the lower right region);
d) Very heavy neutral particle dynamics (the upper right region).

In a similar way, the dynamical behaviours of the particles with variation in the above-mentioned properties can also be explored by moving along the different directions on the plots as discussed below in the four distinctly classified cases as mentioned above.

Case (a): The very light but highly charged positive particles will face high electric but negligible self-gravitational force in the SIP. Such particles will be driven away from there (i.e., region A) towards the region where it will face low electric and high gravitational force (i.e., towards the region B). The high gravity and low electrostatic effects mean condensation of the single particles to form material lumps. For such material lumps, the net-GES force tends to be zero. So, it can be inferred that the very light but highly charged positive particles will follow a way to the near-SSB region in the SIP and form material lumps to balance gravity and electrostatic effects eventually. It is also noticed that such drifting nature of the SIP material decreases towards the SSB due to increasingly well balancing nature of the self-gravity and electrostatic forces. However, a negative ionic particle will follow the just opposite behaviour. They will

travel from the region B (i.e., near-SSB location) to the region A. Such particles will be unable to form material lumps due to low self-gravity environment in the region A. This conclusion again matches with the result already discussed in case of figure 5.10(b). It shows that the presence of very massive negative ions ($m_i/m_- \sim 10^{-2}$) is not a favourable factor in the SIP towards the formation of the realistic GES equilibrium structure explained earlier (figure 5.10(b)). It is noteworthy to mention here again that this result is in agreement with observation as the H^- ion (the lightest) accounts for a major part of the continuous absorption of the solar atmosphere due to its high population density. Other negative ions (rare) have been identified later with advanced spectrophotometric analytical techniques, as in the widely available literature [9, 10].

Case (b): It is further found that very light and neutral particles are almost in a steady state because of the exact gravito-electrostatic force-balancing. Such a situation always appears in the near-heliocentric region. But, with an increase in the positive charge of the lighter particles, they drift more and more towards the near-SSB region and vice-versa (as explored above in the Case (a)).

Case (c): The very heavy and also highly charged positive particles are almost in a steady-state. Such a situation again appears in the near-SSB region. But with a decrease either in charge or mass, they start drifting more and more towards the region B. This movement of positive ions is opposite to that of negative ions in the SIP.

Case (d): The very heavy but neutral particles fall freely under self-gravity action (region C). Such a situation appears in the near-SSB region. But with either increase in positive charge or decrease in mass, they are less drifted towards the region B and vice-versa.

From figure 6.4, it is seen that the magnitudes of the self-gravitational field along the gravity axis increase with a decrease in the δ-value and vice-versa. This behavioural trend is in accord with the SSB formation (with the maximum self-gravity) behaviour with the δ-variation (as in figure 6.1(a)). The region of gravito-electrostatic equilibrium (i.e., region B) signifies the scenarios of the near-SSB region. This SSB region appears within the diagonal zone, characterizing the zero-value of the net GES-force, when all δ-specific plots are combined together simultaneously.

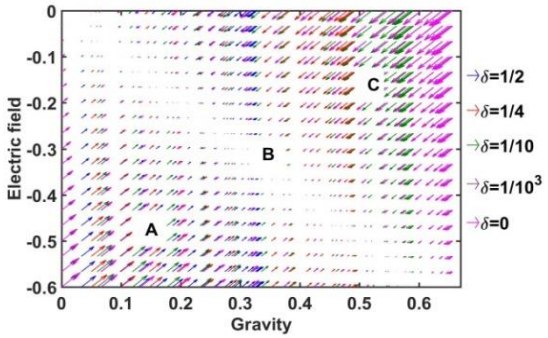
Electric field
Gravity
A
B
C
→δ=1/2
→δ=1/4
→δ=1/10
→δ=1/10^3
→δ=0

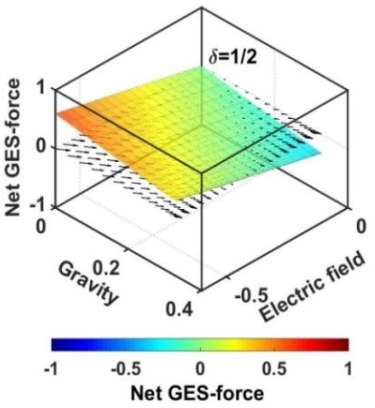
δ=1/2
Net GES-force
Gravity
Electric field
Net GES-force

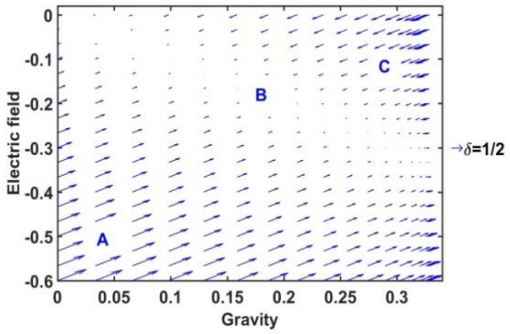
Electric field
Gravity
A
B
C
→δ=1/2

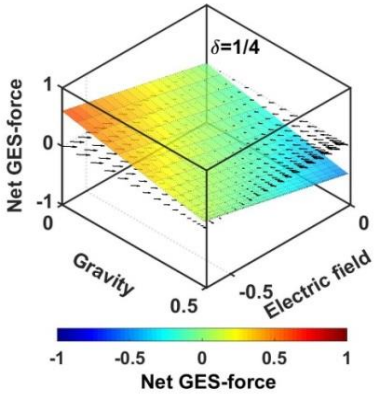
δ=1/4
Net GES-force
Gravity
Electric field
Net GES-force

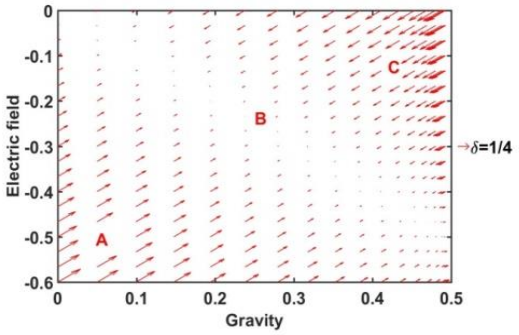
Electric field
Gravity
A
B
C
→δ=1/4

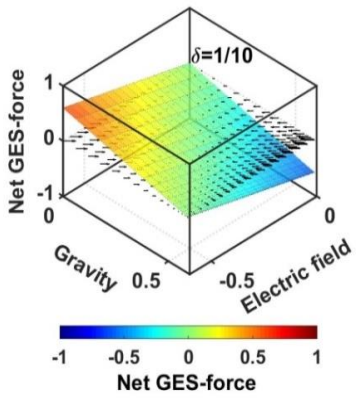
δ=1/10
Net GES-force
Gravity
Electric field
Net GES-force

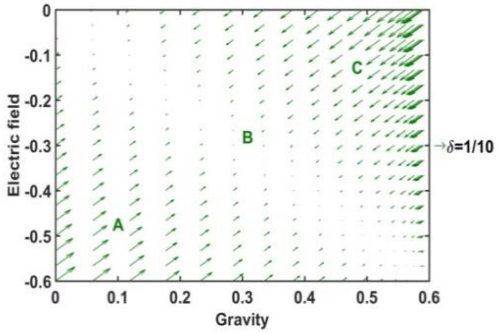
Electric field
Gravity
A
B
C
→δ=1/10

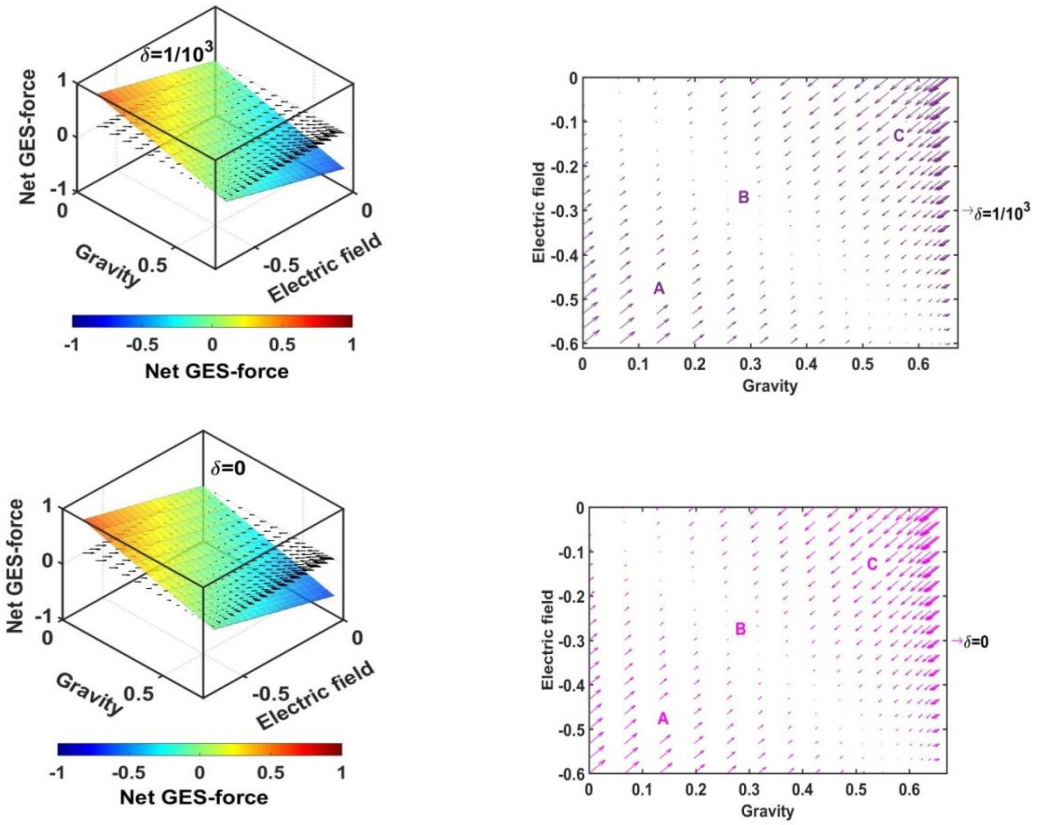

Figure 6.4: *Profile of the net GES-force variation in the SIP with the electric field and self-gravity strength for different values of the equilibrium negative-to-positive ion density ratio (δ) with fixed $m_i/m_- =1$, $T_i/T_e =1$ and $T_-/T_e =1$.*

Again, as evident from figure 6.5, it is inferred that the net GES-force pattern is insensitive to the increasing negative ion mass (figure 6.1(b)). It may be due to their very less population compared to the positive ion population. As a result, the overall particle drifting behaviour, and hence the SIP-material structurization is independent of the mass of the constitutive negative ionic species.

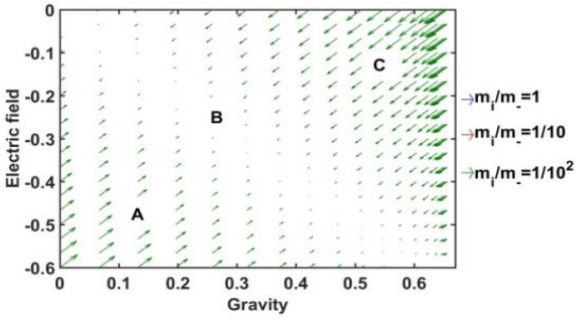

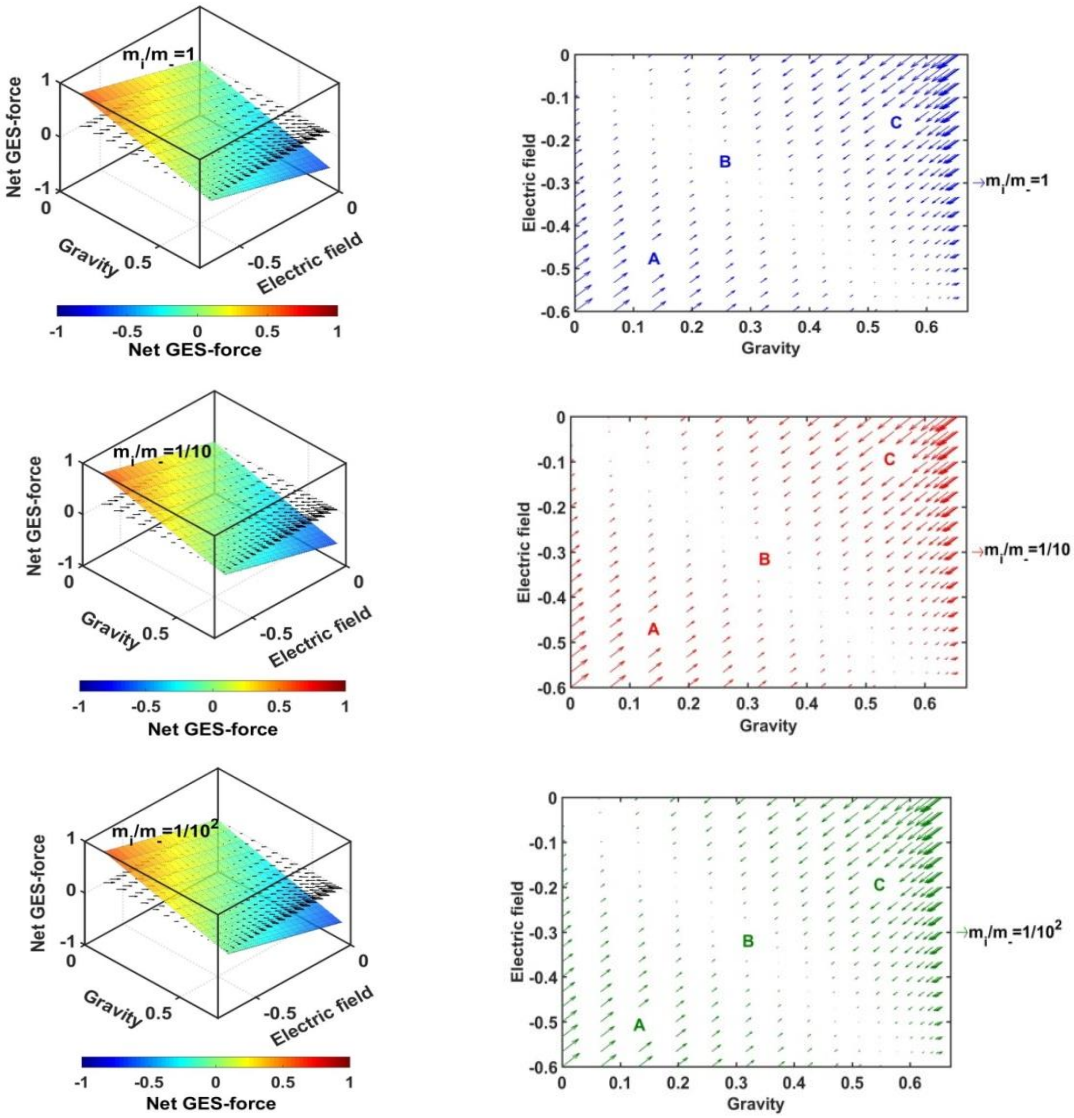

Figure 6.5: *Profile of the net GES-force variation in the SIP with the electric field and self-gravity strength for different values of the positive-to-negative ion mass ratio (m_i/m_-) with fixed $\delta=1/1000$, $T_i/T_e=1$ and $T_-/T_e=1$.*

From figure 6.6, it is clear again that the net GES-force variation behaviour is insensitive to the variation in the positive ion-to-electron temperature ratio (as previously found in figure 6.1(c)). So, the degree of inter-particle collision that is induced by the high positive ionic temperature, does not affect the particle drifting and hence self-structurization in the bounded SIP medium of the present formalism.

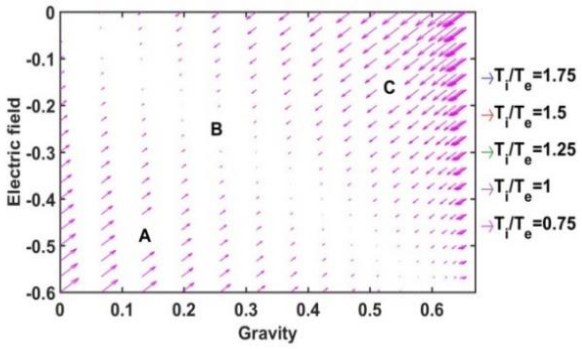
Electric field
Gravity
A
B
C
→T_i/T_e=1.75
→T_i/T_e=1.5
→T_i/T_e=1.25
→T_i/T_e=1
→T_i/T_e=0.75

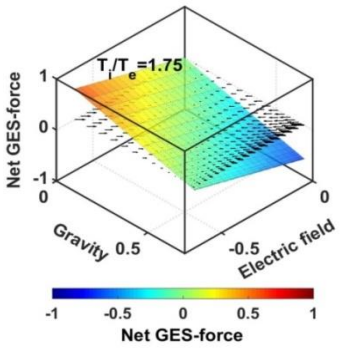
T_i/T_e=1.75
Net GES-force
Gravity
Electric field
Net GES-force

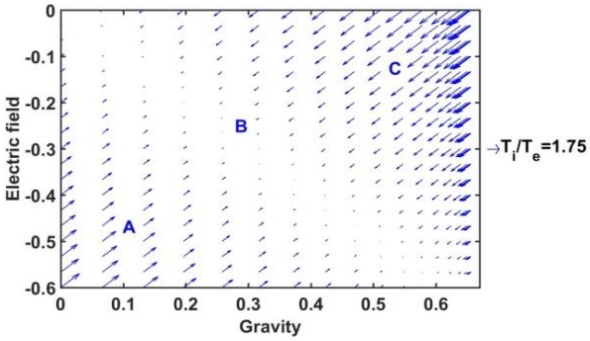
Electric field
Gravity
A
B
C
→T_i/T_e=1.75

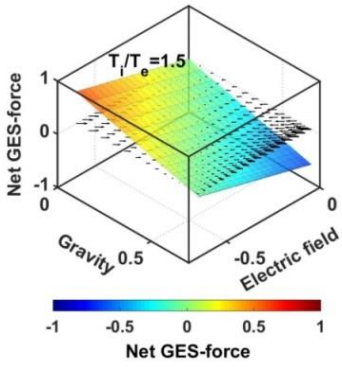
T_i/T_e=1.5
Net GES-force
Gravity
Electric field
Net GES-force

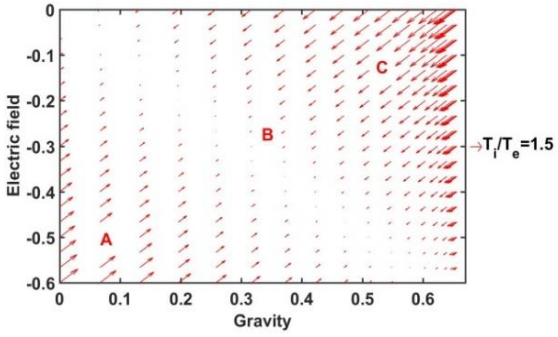
Electric field
Gravity
A
B
C
→T_i/T_e=1.5

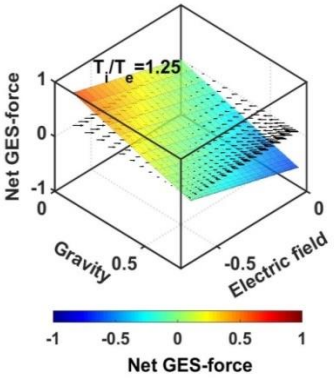
T_i/T_e=1.25
Net GES-force
Gravity
Electric field
Net GES-force

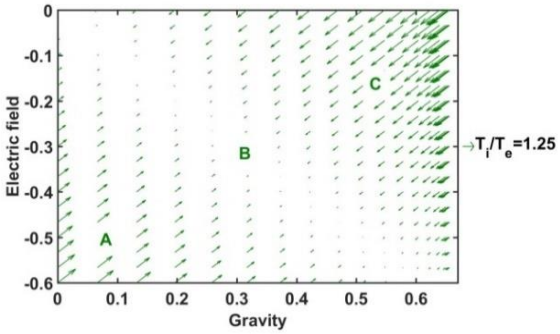
Electric field
Gravity
A
B
C
→T_i/T_e=1.25

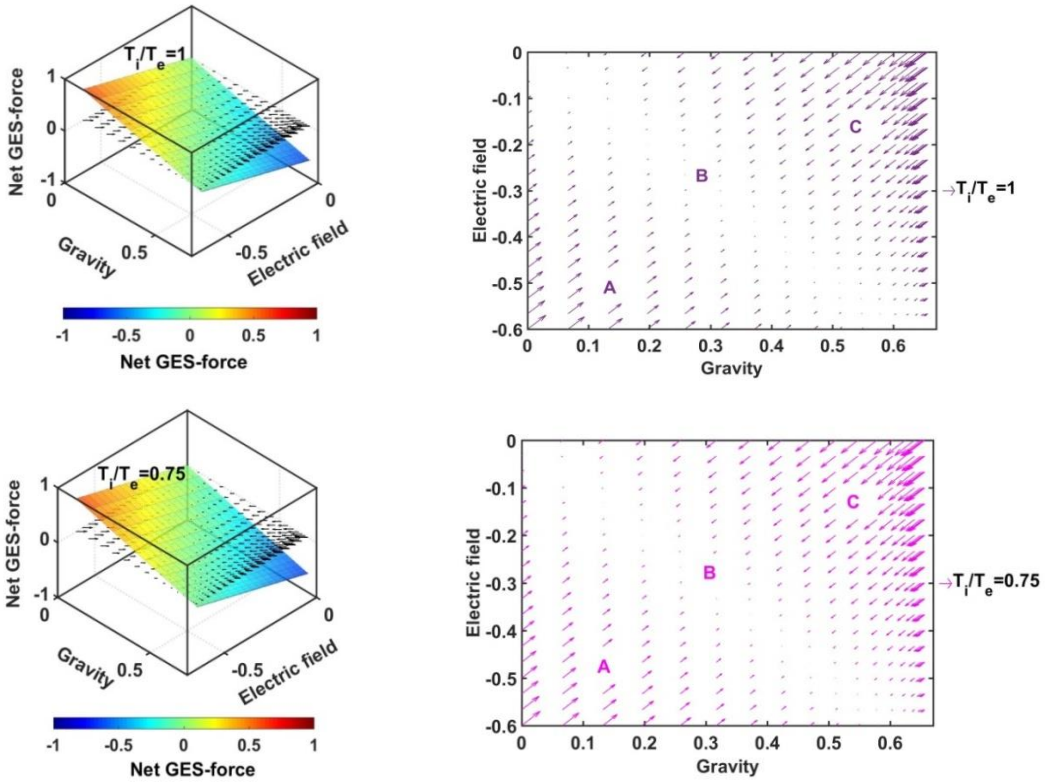

Figure 6.6: *Profile of the net GES-force variation in the SIP with the electric field and self-gravity strength for different values of the positive ion-to-electron temperature ratio (T_i/T_e) with fixed δ=1/1000, m_i/m_-=1 and T_-/T_e=1.*

It is seen in figure 6.7 that the net GES-force variation with its electric and gravitational field is insensitive to the negative ion-to-electron temperature ratio (as previously found in figure 6.1(d)). So, the degree of inter-particle collision, which is induced by the high negative ionic temperature, does not affect the particle drifting and hence self-structurization in the SIP.

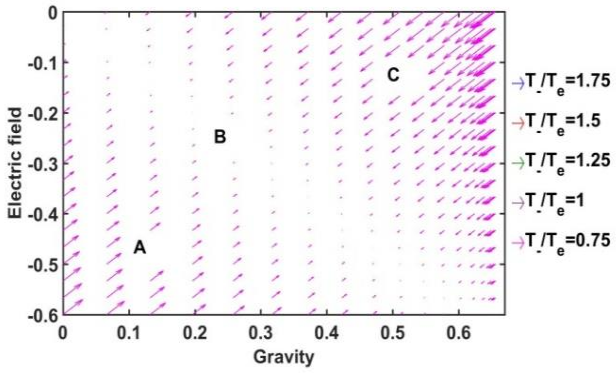

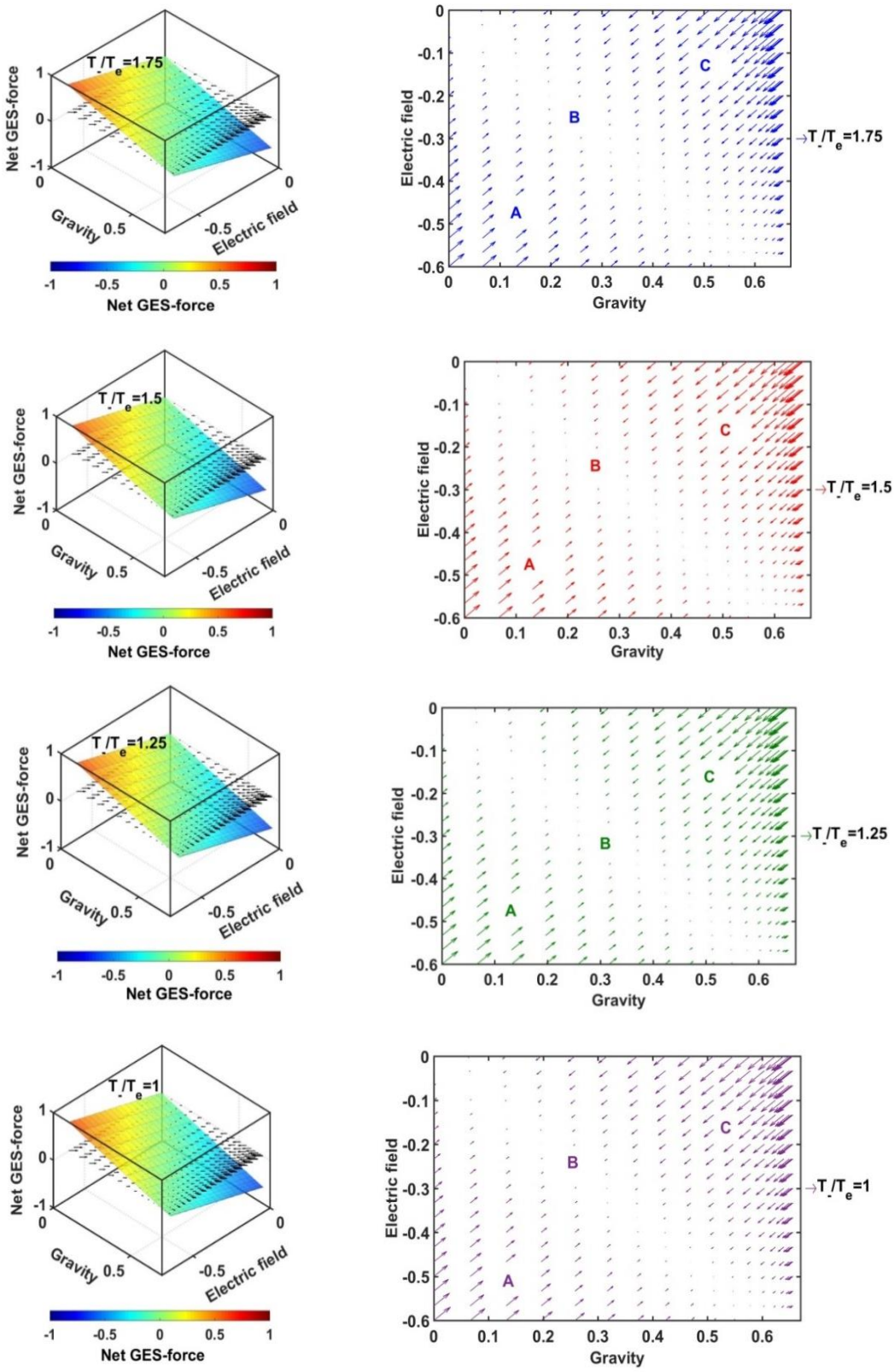
T-/Te=1.75
Net GES-force
Gravity
Electric field
Net GES-force
A
B
C
Electric field
Gravity
→T-/Te=1.75
T-/Te=1.5
Net GES-force
Gravity
Electric field
Net GES-force
A
B
C
Electric field
Gravity
→T-/Te=1.5
T-/Te=1.25
Net GES-force
Gravity
Electric field
Net GES-force
A
B
C
Electric field
Gravity
→T-/Te=1.25
T-/Te=1
Net GES-force
Gravity
Electric field
Net GES-force
A
B
C
Electric field
Gravity
→T-/Te=1

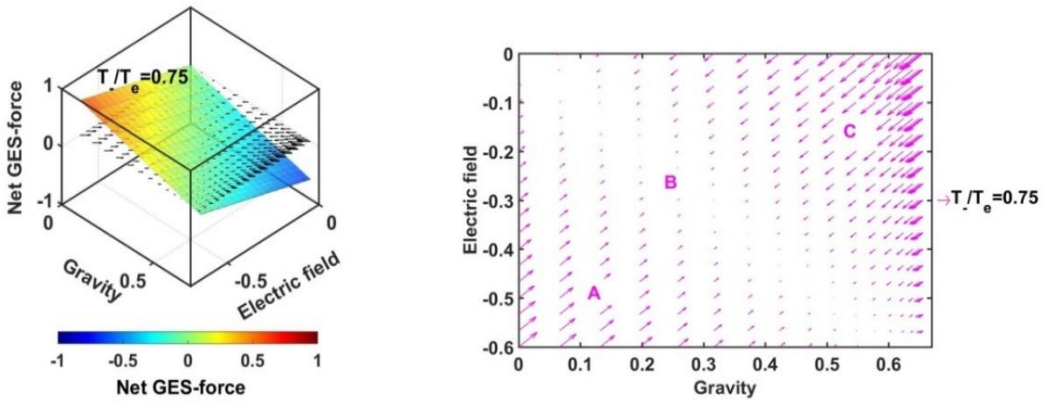

Figure 6.7: *Profile of the net GES-force variation in the SIP with the electric field and self-gravity strength for different values of the negative ion-to-electron temperature ratio (T_-/T_e) with fixed $\delta=1/1000$, $m_i/m_-=1$ and $T_i/T_e=1$.*

6.4 CONCLUSIONS

This theoretical exploration illuminates the equilibrium solar plasma elemental flow behaviours in the field of gravito-electrostatic interaction in the modified GES model framework. The model is refined methodically by a proper inclusion of the realistic negative ionic effects for the first time [4, 5]. The spherical solar plasma volume is assumed to be made up of inertialess electrons following Boltzmann-distribution, gravito-electrostatically coupled with positive and negative ionic inertial fluids, via the Poisson equations. The basic model-governing equations for the tri-component plasmas are accordingly followed for the SIP scale dynamics. The numerical analysis reveals the boundary of the confined solar plasma where the net-GES force vanishes (figure 6.1).

The plasma constitutive material self-organization, and hence, inhomogeneity in the SIP mass and the net electric charge distribution are studied with the radial gradient variation of the self-gravity and electric field strengths (figures 6.2-6.3). Interestingly, a location with δ-insensitive gravity gradient is revealed in the SIP. The dynamical behaviours of the constituent plasma elements with variation in their mass and electric charge are elaborately investigated in the defined gravito-electrostatic interaction phase space. In the SIP, the positive ions have a tendency to move towards the region of high self-gravity and low electrostatic effects. The opposite is the case for the negative ones. It, indeed, clearly portrays the solar material clumping nature in the SIP. This atypical clumping behaviour, reported herewith for the first time (figures 6.4-6.7), clearly matches with the observational results in the respect that the heavy negative ion formation (against the lighter ones) is not favoured in the confined SIP medium [9, 10].

REFERENCES

[1] Stix, M. *The Sun: An Introduction*. Springer, Berlin, 1991.

[2] Priest, E. *Magnetohydrodynamics of the Sun*. Cambridge University Press, Cambridge, New York, 2014.

[3] Kippenhahn, R., Weigert, A., and Weiss, A. *Stellar Structure and Evolution*. Springer, Berlin, 2012.

[4] Wildt, R. Negative ions of hydrogen and the opacity of stellar atmospheres. *Astrophysical Journal*, 90:611-620, 1939.

[5] Millar, T. J., Walsh, C., and Field, T. A. Negative ions in space. *Chemical Reviews*, 117(3):1765–1795, 2017.

[6] Dwivedi, C. B., Karmakar, P. K., and Tripathy, S. C. A gravito-electrostatic sheath model for surface origin of subsonic solar wind plasma. *Astrophysical Journal*, 663:1340-1353, 2007.

[7] Gilat, A. *MATLAB: An Introduction with Applications*. Wiley, NJ, 2011.

[8] Goutam, H. P. and Karmakar, P. K. Turbulent gravito-electrostatic sheath (GES) structure with kappa-distributed electrons for solar plasma characterization. *Solar Physics*, 292:182 (1)-182(12), 2017.

[9] Branscomb, L. M. and F. Pagel, B. E. Atomic and molecular negative ions in stellar atmospheres. *Monthly Notices of the Royal Astronomical Society*, 118:258-270, 1958.

[10] Vardya, M. S. Role of negative ions in late-type stars. *Memoirs of the Royal Astronomical Society*, 71:249-269, 1967.